RSC Advances

PAPER

View Article Online
View Journal | View Issue

Cite this: *RSC Adv.*, 2017, **7**, 30392

Fabrication of metal/semiconductor hybrid Ag/$AgInO_2$ nanocomposites with enhanced visible-light-driven photocatalytic properties

Xiangchao Zhang, *[a] Difa Xu,[a] Yanrong Jia[ab] and Shiying Zhang*[a]

Recently, exploration of the potential application of heterogeneous photocatalysis has attracted significant interest in the fields of environmental remediation and energy conversion. The metal–semiconductor hybrid nanostructures play very important roles in solar-to-chemical energy conversion due to their unique optical characteristics and catalytic properties. In this study, a novel photocatalyst constructed using Ag and $AgInO_2$ was developed to improve the visible-light-driven properties. The photocatalytic efficiency of Ag/$AgInO_2$ for the degradation of methylene blue (MB) reached 97.8%, which was much higher than that of pure $AgInO_2$. Characterization results show that the as-prepared nanocomposites can not only broaden the visible-light absorption range but also promote the separation of the photogenerated electron–hole pairs. Trapping experiments confirmed that superoxide radicals ($^{\bullet}O^{2-}$) and holes (h^+) were the predominant contributors in the degradation of the organic dye MB. These encouraging results provide an alternative approach for the development of metal–semiconductor hybrid nanostructures towards improving the efficiency of solar-energy utilization in the near future.

Received 24th February 2017
Accepted 23rd May 2017

DOI: 10.1039/c7ra02331f

rsc.li/rsc-advances

1. Introduction

Nowadays, harnessing of the solar energy to chemical energy conversion *via* photocatalysis is one of the hottest research topics because of its potential to solve increasingly serious energy shortages and environmental pollution problems.[1] Undoubtedly, semiconductor-based heterogeneous photocatalysis, as a green and sustainable technology, continues to attract significant attention due to its substantial progress in water and air pollution treatment, H_2 generation and CO_2 conversion, and artificial photosynthesis.[2–4] In the perspective of efficient utilization of solar light, extensive efforts have been devoted to the exploration of visible-light-driven photocatalysts for environmental and energy-related applications. To date, several types of oxides, sulfides, nitrides, and other photocatalysts have been developed.[5–8] However, the efficiency of the existing photocatalysts is restricted by the low absorption capacity and/or the fast charge carrier recombination to meet the requirements of commercial applications. Thus, it is particularly important to explore an efficient strategy for the design and preparation of advanced photocatalytic materials with high efficiencies.

In the past decade, Ag-based photocatalysts have been rapidly developed, which have been proven to be one of the most attractive candidates with high photocatalytic efficiency under visible-light irradiation.[9] On the other band, exploration of an efficient strategy to improve the photocatalytic performances remains a great challenge; one of the efficient approaches include the combination of noble metal co-catalysts (such as silver and gold) with semiconductors to construct nanocomposites.[10] Furthermore, the hybrid between a semiconductor and a metal can produce an active interface and enhance the interfacial charge separation.[11] Some studies have reported that the metal/semiconductor hybrid photocatalysts, such as Ag/$AgPO_3$, Ag/$SrTiO_3$, Au/$CdMoO_4$, Ni/CdS, and Bi/$ZnWO_4$, have achieved important higher reaction rates in various photocatalytic reactions compared to their pristine counterparts.[12–18] After this, Zhang *et al.* mentioned that despite the importance of Ag/semiconductor composites in heterogeneous photocatalysis, the interplay between Ag and semiconductors still remained largely unexplored.[19] In our previous studies,[20,21] our group has reported Ag/$AgAlO_2$ composites and Ag/$AgGaO_2$ metal–semiconductor heterostructures with the enhanced photocatalytic activities under visible-light irradiation. Based on the abovementioned studies, $AgInO_2$, which belongs to the family of $AgMO_2$ (M = Al, Ga, and In), is another promising Ag-based photocatalyst containing d_{10} metal ion electronic configuration of Ag^+; however, to the best of our knowledge, to date, no study has been reported on the preparation of the Ag/$AgInO_2$ nanocomposites as an efficient visible-light-responsive photocatalyst for organic dye decomposition.

Herein, we developed a novel metal–semiconductor hybrid of Ag/$AgInO_2$ nanocomposites through a three-step method.

[a]*Hunan Key Laboratory of Applied Environmental Photocatalysis, Changsha University, Changsha, Hunan 410022, P. R. China. E-mail: xczhang@ccsu.edu.cn; cdzhangshiying@163.com; Fax: +86-731-8426-1208; Tel: +86-731-8426-1297*
[b]*Jiangsu Hengshen Co., Ltd., Danyang, Jiangsu, 212314, P. R. China*

The microstructure and optical properties of the as-prepared samples were investigated using XRD, SEM, EDS, TEM/HRTEM, XPS, PL, and UV-vis absorption spectra. The photocatalytic properties of the $Ag/AgInO_2$ nanocomposites were evaluated by the photodegradation of an organic dye pollutant, MB solution, under visible-light irradiation. Compared to $AgInO_2$, the $Ag/AgInO_2$ nanocomposites exhibited superior photocatalytic activities. The proposed photocatalytic mechanism has also been discussed.

2. Experimental

2.1 Material preparation

All the chemicals were of analytical grade and used throughout the experiments without further purification. Since Ag_2O decomposes at a temperature higher than 300 °C, it poses great challenges for the synthesis of silver compounds in a single-step *via* conventional solid-state reaction.[22] A schematic of the preparation of the $Ag/AgInO_2$ nanocomposite was proposed by the three-step method, as shown in Fig. 1. Typically, the precursor $NaInO_2$ was synthesized *via* a solid-state reaction. Next, 0.01 mol In_2O_3 and 0.01 mol Na_2CO_3 were mixed and then sintered at 800 °C for 5 h to obtain the white $NaInO_2$ powder. Second, the $AgInO_2$ sample was prepared by an ion exchange method, which was carried out by heating the mixture of $NaInO_2$, $AgNO_3$, and KNO_3 with a molar ratio of 1.0 : 1.5 : 1.0 at 220 °C for 10 h. Third, the hybrid $Ag/AgInO_2$ products were fabricated through the thermal decomposition of the excess $AgNO_3$ at 350 °C for 60 min to ensure the intimate contact between Ag and $AgInO_2$. Finally, the precipitates were repeatedly washed with distilled water and dried at 80 °C in air for 5–8 h.

2.2 Sample characterization

The crystalline structure of the as-obtained samples was determined using a Bruker AXS D8 Advance X-ray diffractometer with Cu Kα radiation ($\lambda = 0.15406$ nm) in the 2θ range from 10° to 70°. The morphological characteristics and microstructures of the products were examined by field-emission scanning electron microscopy (FESEM; equipped with energy-dispersive X-ray spectroscopy (EDS), JEOL model JSM-6360LV) and high-resolution transmission electron microscopy (HRTEM, JEM-3010). The ultraviolet-visible (UV-vis) absorption spectra were acquired by a UV-vis spectrometer (UV-2450, Shimadzu) in the range from 200 to 700 nm using $BaSO_4$ as the reference. Photoluminescence (PL) spectra were obtained using a fluorescence spectrophotometer (F-7000, Hitachi, Japan). X-ray photoelectron spectroscopy (XPS) measurement was performed using a spectrometer (Kratos AXIS Ultra DLD) equipped with an Al Kα X-ray radiation source. The XPS binding energy (BE) was internally referenced to the C 1s peak (BE = 284.6 eV).

2.3 Evaluation of the properties

Photocatalytic activities of the as-prepared samples were evaluated by the degradation of MB under visible-light irradiation. The light source was a 300 W xenon lamp with a 400 nm cut-off filter. Experimental details have been previously published.[21,23] Briefly, the photocatalytic reaction was carried out in an open reactor containing 200 mL of MB solution at a concentration of 10 mg L^{-1} and 0.2 g catalyst. Prior to irradiation, the solution suspension was magnetically stirred for 30 min to ensure adsorption/desorption equilibrium between the samples and MB solution in the dark. Every 30 min, we took out about 4 mL of suspension to analyze the MB concentration, which was tested by a Shimadzu UV-2450 spectrophotometer. The maximum absorption peak of MB was at $\lambda = 664$ nm. The degradation rate D was calculated as $D = (C_0 - C_t)/C_0 \times 100\%$, where C_0 and C_t are the MB concentrations at initial state and after irradiation for t min, respectively.

3. Results and discussion

The composition and crystallographic structure of the as-synthesized $NaInO_2$, $AgInO_2$, and $Ag/AgInO_2$ composites were confirmed by the XRD patterns, as shown in Fig. 2.

It was observed that the sharp diffraction peaks of the precursor can be well indexed as $NaInO_2$ (JPCDS no. 65-3663). No diffraction peaks of the raw materials and other impurities were observed, indicating that the as-prepared samples were pure $NaInO_2$ under the proposed conditions. The XRD pattern of $AgInO_2$ shows typical diffraction peaks 2θ located at 14.0°, 28.3°, 32.9°, 36.9°, 50.3°, 56.1°, 58.6°, 64.0°, and 66.6°, corresponding to (003), (006), (012), (104), (018), (110), (0012), (116), and (202), respectively, which are well-indexed to the rhombohedral structure of $AgInO_2$ with JCPDS no. 21-1077 (space group of $R3m$ and calculated cell parameters $a = b = 3.277$ Å and $c = 18.877$ Å), suggesting that pure-phase $AgInO_2$ is formed and well crystallized through an ion exchange reaction. For $Ag/AgInO_2$,

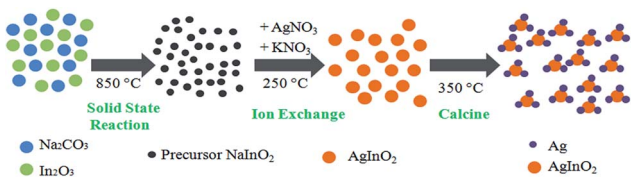

Fig. 1 Schematic of the fabrication of the $Ag/AgInO_2$ metal–semiconductor hybrid.

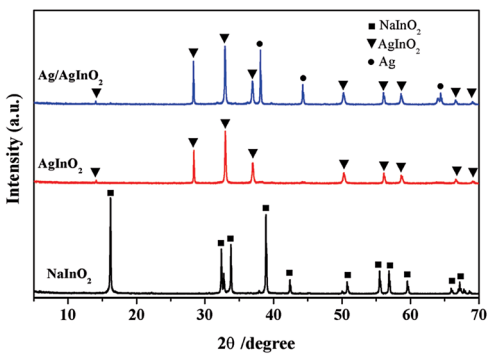

Fig. 2 XRD patterns of the as-synthesized samples.

besides the peaks of $AgInO_2$, the major diffraction peaks of the metal Ag (JCPDS no. 65-2871) are also present. Therefore, it is speculated from the XRD results that the nanocomposite based on the hybrid of metal Ag with semiconductor $AgInO_2$ has been successfully prepared by the abovementioned three-step method.

The morphologies of the representative samples were determined using SEM and TEM/HRTEM. As shown in Fig. 3, no uniform morphologies were obtained in our experiment due to the preparation method, and the as-synthesized $NaInO_2$, $AgInO_2$, and $Ag/AgInO_2$ samples were composed of irregular particles with the diameters about dozens to hundreds of nm in addition to a certain degree of agglomeration. The microstructures are the typical structures obtained from the solid-state method. EDS analysis in Fig. 2(d) shows that the atomic ratio of In : Ag : O is 1.0 : 1.17 : 2.27. It is worth noticing that the molar ratio of Ag to In for the $Ag/AgInO_2$ sample is 1.17 : 1, which is higher than that in $AgInO_2$ (1 : 1). From the HRTEM images of the $Ag/AgInO_2$ composites in Fig. 2(f), two lattice fringes at about 0.31 nm and 0.24 nm can be distinctly identified, in agreement with the spacing of the (006) plane of silver delafossite $AgInO_2$ and the (111) plane of cubic Ag, respectively. Note that a heterojunction structure can be clearly observed between $AgInO_2$ and Ag. This corresponds well with the results of the XRD as discussed above, which also lends support to the formation of Ag-loaded $AgInO_2$.

The optical properties of the pure $AgInO_2$ and $Ag/AgInO_2$ composites are shown in Fig. 4. As presented in the UV-vis absorption spectra in Fig. 4(a), it is clearly observed that both samples exhibit visible-light absorption in the range of 400–600 nm. In the case of the $Ag/AgInO_2$ composite, the absorbance in the range of 400–700 nm is higher than that of pure $AgInO_2$, which is attributed to the characteristic absorption of surface plasmon resonance (SPR) of metallic silver on the $AgInO_2$ surface.[13] The SPR effect of Ag can enhance the captured electron energy and transfer rate. The band gap energy (E_g) of the catalysts can be estimated according to the transformed Kubelka–Munk function obtained from a plot of light energy $(\alpha h\nu)^{1/2}$ *versus* photon energy $h\nu$. The indirect band gap of $AgInO_2$ was evaluated to be 2.46 eV. Furthermore, an interesting finding is that the absorption edge of the $Ag/AgInO_2$ composite shows an obvious red-shift and enhanced absorption in the visible light range was observed due to introduction of the metal Ag. These results imply that the extension towards longer wavelength and enhanced visible-light absorption of the hybrid $Ag/AgInO_2$ can generate more available photogenerated carriers, thus favoring the photocatalytic activities for the degradation of the organic dye MB wastewater. On the other hand, because the PL emission results from the recombination charge carriers, the PL spectra of the semiconductors are useful to disclose the migration, transfer, and recombination processes of the photogenerated electron–hole pairs.[24,25] Fig. 4(c) shows the PL spectra of the pure $AgInO_2$ and $Ag/AgInO_2$ composites under the excitation wavelength of 254 nm. From the results, it can be observed that the PL intensity of the $Ag/AgInO_2$ sample becomes weaker as compared to that of the pure $AgInO_2$, indicating that the $Ag/AgInO_2$ hybrid can efficiently slow down the recombination of the photogenerated carriers; this is beneficial to the superior photocatalytic properties of the $Ag/AgInO_2$ composites under visible light irradiation.

The photocatalytic properties of the $AgInO_2$ and $Ag/AgInO_2$ samples were determined using MB dye as a target contaminant of wastewater. Fig. 5(a) shows the degradation rates of the MB solution in the presence of different samples. It was observed

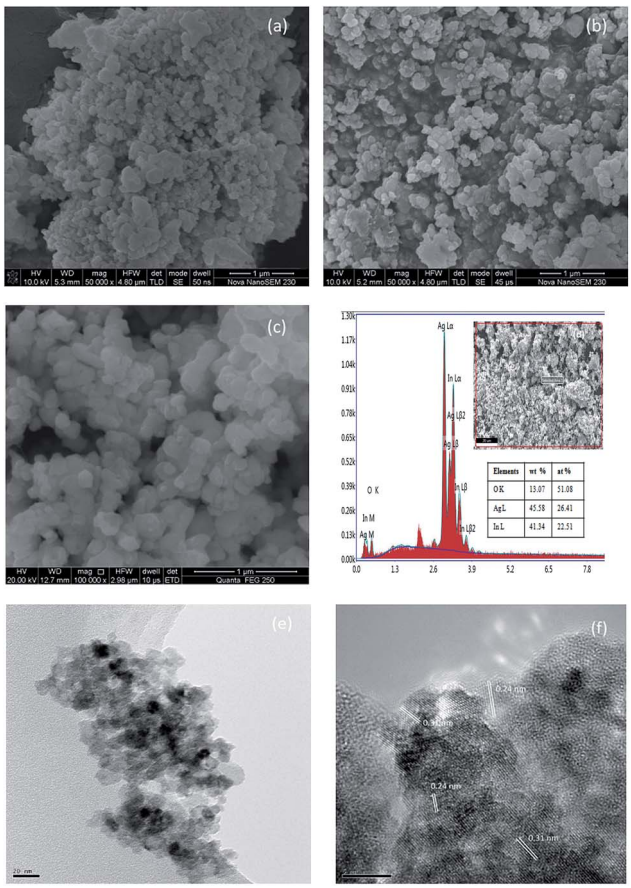

Fig. 3 Morphologies of the samples: (a) SEM images of the precursor $NaInO_2$, (b) SEM images of the pure $AgInO_2$, (c) SEM images of the $Ag/AgInO_2$ composites, (d) EDS spectra of the $Ag/AgInO_2$ hybrid (inseted profile: the selected area from SEM and EDS results), (e) TEM images of the $Ag/AgInO_2$ composites, and (f) HRTEM images of the $Ag/AgInO_2$ composites.

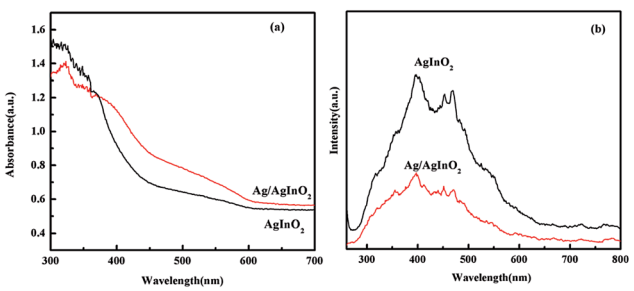

Fig. 4 Optical properties of the pure $AgInO_2$ and $Ag/AgInO_2$ composites: (a) UV-vis absorption spectra and (b) PL spectra with excitation wavelength of 254 nm.

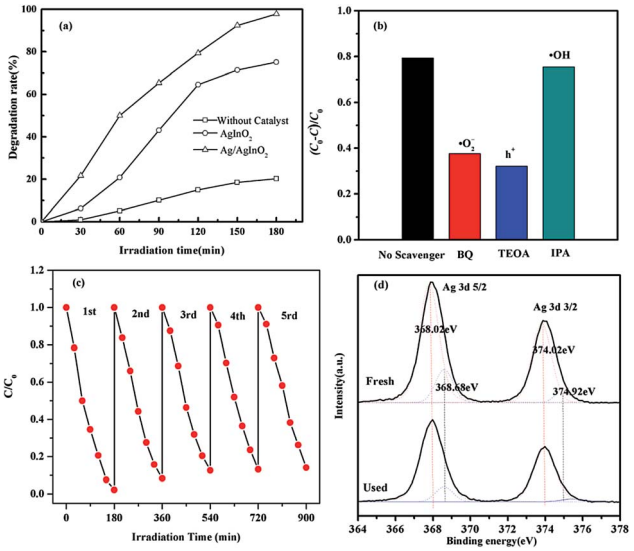

Fig. 5 The photocatalytic properties for the (a) degradation rates of MB solution in the presence of different samples, (b) photocatalytic degradation efficiency of MB with selected scavengers in the presence of $Ag/AgInO_2$ after 120 min of visible-light illumination, (c) reusability of $Ag/AgInO_2$ nanocomposites under visible light irradiation, and (d) high-resolution XPS spectra of Ag 3d of the $Ag/AgInO_2$ samples before and after photocatalytic activity tests for the five cycles.

that the percent degradation of MB without a photocatalyst was very slow. The photocatalytic activities of the $Ag/AgInO_2$ composites for the degradation of MB under 3 h visible-light irradiation reached 97.8%, which was much higher than that of the $AgInO_2$ (only 75.1%) catalyst.

Fig. 5(b) shows the results of the active species trapping experiments to investigate the effects of a series of scavengers on the degradation rates of MB. Typically,[26–28] three different chemicals, triethanolamine (TEOA, 0.01 mol L^{-1}), isopropyl alcohol (IPA, 0.02 mol L^{-1}), and *p*-benzoquinone (BQ, 0.1 mmol L^{-1}), were employed as scavengers for photogenerated holes (h^+), hydroxyl radical ($^{\bullet}OH$), and superoxide radicals ($^{\bullet}O^{2-}$), respectively. The comparative experiment with no scavenger was also performed under identical conditions. It can be seen that there is only a slight decrease in the presence of IPA, indicating that the effect of hydroxyl radical ($^{\bullet}OH$) on the photocatalytic degradation of MB by $Ag/AgInO_2$ composites is negligible under visible-light irradiation. The photocatalytic degradation of MB remarkably decreases after adding TEOA, suggesting that holes (h^+) are the main active species during the photocatalytic process. When BQ is added, the degradation efficiency of dye also decreases to 37.59%. It means that superoxide radical ($^{\bullet}O^{2-}$) plays an almost equally important role in the photodegradation reaction of MB. Therefore, it can be concluded that h^+ and $^{\bullet}O^{2-}$ are the main active species for the photocatalysis of MB in the presence of the $Ag/AgInO_2$ composites.

The reusability and stability of the Ag-based photocatalysts are the other important factors in the practical applications. The photocatalytic degradation percentage of MB obtained using the $Ag/AgInO_2$ samples under visible-light irradiation in 5 cycles is shown in Fig. 5(c). There was no appreciable loss in the photocatalytic activity of the $Ag/AgInO_2$ hybrid after the five runs; in addition to this, the XPS results, as shown in Fig. 5(d), exhibited that the characteristic peaks of Ag 3d of the recycled $Ag/AgInO_2$ composites were almost similar to those of the fresh composites. It can be concluded that the hybrid $Ag/AgInO_2$ composites possess admirable reusability and photostability even after five cycles for the degradation of MB dye. These encouraging results prove that the $Ag/AgInO_2$ metal–semiconductor hybrid nanostructure can be expected to be a promising candidate in organic dye wastewater purification.

Based on the abovementioned experiment results as well as the ref. 29–36, we proposed the possible mechanism for the enhanced photocatalytic properties for the degradation of MB on a $Ag/AgInO_2$ metal–semiconductor hybrid, as shown in Fig. 6. The band edge positions of the conduction band (CB) and the valence band (VB) of $AgInO_2$ at the point of zero charge could be theoretically calculated by the Mulliken electronegativity theory: $E_{CB} = \chi - E^C - 1/2E_g$. Herein, E_{CB} is the conduction band edge energy and χ is the absolute electronegativity of the semiconductor. E^C is the energy of free electrons in the hydrogen scale (~4.5 eV), and E_g is the band gap energy of the semiconductor. E_{VB} could be obtained by the equation of $E_{VB} = E_{CB} + E_g$. Thus, the values of CB and VB of $AgInO_2$ were predicted to be −0.44 eV and 2.02 eV, respectively. When the $Ag/AgInO_2$ composites are irradiated under visible light, the photogenerated electrons of $AgInO_2$ can be excited from the VB to the CB; moreover, the holes stay at the VB to directly oxidize MB to degradation products because the VB potential of $AgInO_2$ is more positive than the standard redox potential of $^{\bullet}OH/OH^-$ (1.99 V *vs.* NHE), and h^+ can directly oxidize OH^- to generate $^{\bullet}OH$ radicals in the $AgInO_2$ photocatalytic system. The as-produced $^{\bullet}OH$ radicals can then degrade MB into CO_2 and H_2O. On the other hand, metallic Ag can also absorb visible light due to the SPR effect, and the absorbed photons would be efficiently separated into an electron and a hole. Moreover, an inner electromagnetic field can promote the higher separation efficiency of the photoproduced carriers when the metal Ag and the semiconductor $AgInO_2$ are in direct contact. As a result, the photogenerated electrons on the Ag surface can be trapped by absorbed O_2 in the solution to produce superoxide radical

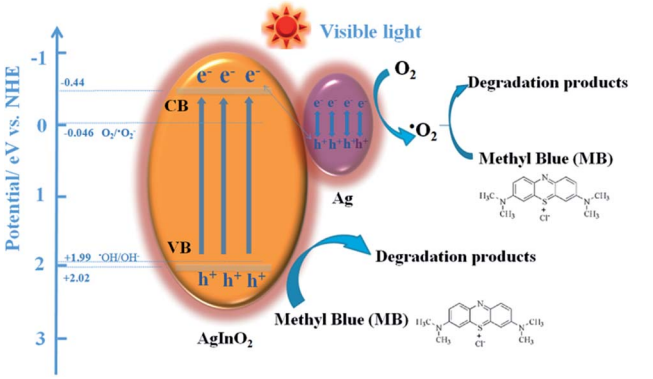

Fig. 6 Schematic of the proposed mechanism for the degradation of MB on a $Ag/AgInO_2$ metal–semiconductor hybrid.

($^{\cdot}O^{2-}$). These active species are strong oxidants that can photocatalyze MB to the degradation products. The proposed process can be described as follows:

$$AgInO_2 + h\nu \rightarrow AgInO_2(h^+) + AgInO_2(e^-) \quad (1)$$

$$Ag + h\nu \rightarrow Ag(h^+) + Ag(e^-) \quad (2)$$

$$O_2 + e^- \rightarrow {}^{\cdot}O^{2-} \quad (3)$$

$$h^+ + MB \rightarrow \text{degradation products} \quad (4)$$

$$^{\cdot}O^{2-} + MB \rightarrow \text{degradation products} \quad (5)$$

4. Conclusions

In conclusion, a novel $Ag/AgInO_2$ metal–semiconductor hybrid nanostructure was designed and synthesized. The as-prepared $Ag/AgInO_2$ nanocomposites exhibited enhanced photocatalytic activity (97.8%) for the degradation of MB as compared to that of a bare $AgInO_2$ catalyst (75.1%). The UV-vis absorption spectra results indicated that the absorption edge of the $Ag/AgInO_2$ composite showed an obvious red-shift and enhanced absorption in the visible-light range was observed. PL spectra demonstrated that the incorporation of the metal Ag onto the $AgInO_2$ surface promoted the separation of the photogenerated carriers. The active species trapping experiments concluded that h^+ and $^{\cdot}O^{2-}$ were the main active species in the photocatalysis of MB in the presence of the $Ag/AgInO_2$ composites. This study provides some insight into the development of metal–semiconductor hybrid nanostructures for enhancing the visible-light-driven photocatalytic properties.

Acknowledgements

This work was supported by the Program for the Hunan Provincial Natural Science Foundation of China (2016JJ6008), Scientific Research Fund of Hunan Provincial Education Department (17B029), and X. Zhang is grateful for the financial support received from the China Scholarship Council (201508430023).

Notes and references

1 X. Meng, L. Liu, S. Ouyang, H. Xu, D. Wang, N. Zhao and J. Ye, *Adv. Mater.*, 2016, **28**, 6781–6803.
2 J. Li, K. Zhao, Y. Yu and L. Zhang, *Adv. Funct. Mater.*, 2015, **25**, 2189–2201.
3 S. Wang, J. Yun, B. Luo, T. Butburee, P. Peerakiatkhajohn, S. Thaweesak, M. Xiao and L. Wang, *J. Mater. Sci. Technol.*, 2017, **33**, 1–22.
4 Z. Li, J. Feng, S. Yan and Z. Zou, *Nano Today*, 2015, **10**, 468–486.
5 X. Li, J. Yu and M. Jaroniec, *Chem. Soc. Rev.*, 2016, **45**, 2603–2636.
6 X. Zhu, P. Wang, B. Huang, X. Ma, X. Qin, X. Zhang and Y. Dai, *Appl. Catal., B*, 2016, **199**, 315–322.
7 S. Guo, X. Li, J. Zhu, T. Tong and B. Wei, *Small*, 2016, **12**, 5692–5701.
8 X. Li, J. Zhu and B. Wei, *Chem. Soc. Rev.*, 2016, **45**, 3145–3187.
9 M. Akhtar, M. Menon, M. Sunkara, G. Sumanasekera, A. Durygin and J. Jasinski, *J. Alloys Compd.*, 2015, **641**, 87–92.
10 J. Bi, Z. Zhou, M. Chen, S. Liang, Y. He, Z. Zhang and L. Wu, *Appl. Surf. Sci.*, 2015, **349**, 292–298.
11 P. Bermel, K. Yazawa, J. Gray, X. Xu and A. Shakouri, *Energy Environ. Sci.*, 2016, **9**, 2776–2788.
12 H. Dong, Z. Li, X. Xu, Z. Ding, L. Wu, X. Wang and X. Fu, *Appl. Catal., B*, 2009, **89**, 551–556.
13 Q. Zhang, Y. Huang, L. Xu, J. Cao, W. Ho and S. Lee, *ACS Appl. Mater. Interfaces*, 2016, **8**, 4165–4174.
14 F. Tian, H. Zhao, G. Li, Z. Dai, Y. Liu and R. Chen, *ChemSusChem*, 2016, **9**, 1579–1585.
15 D. Chen, Q. Chen, L. Ge, L. Yin, B. Fan, H. Wang, H. Lu, H. Xu, R. Zhang and G. Shao, *Appl. Surf. Sci.*, 2013, **284**, 921–929.
16 Y. Gao, Y. Huang, Y. Li, Q. Zhang, J. Cao, W. Ho and S. Lee, *ACS Sustainable Chem. Eng.*, 2016, **4**, 6912–6920.
17 O. Acuña, H. Villavicencio, V. Petranovskii and O. Herrera, *Catal. Commun.*, 2016, **75**, 103–107.
18 S. Ouyang, N. Kikugawa, D. Chen, Z. Zou and J. Ye, *J. Phys. Chem. C*, 2009, **113**, 1560–1566.
19 T. Zhang, W. Lei, P. Liu, J. Rodriguez, J. Yu, Y. Qi, G. Liu and M. Liu, *J. Phys. Chem. C*, 2016, **120**, 2777–2786.
20 X. Zhang, Z. Luo, Y. Wang and S. Zhang, *Chem. Lett.*, 2016, **45**, 1288–1290.
21 X. Zhang, A. Tang, Y. Jia, Y. Wang, H. Wang and S. Zhang, *J. Alloys Compd.*, 2017, **701**, 16–22.
22 H. Dong, Z. Li, X. Xu, Z. Ding, L. Wu, X. Wang and X. Fu, *Appl. Catal., B*, 2009, **89**, 551–556.
23 K. Xu, D. Xu, X. Zhang, Z. Luo and S. Zhang, *Appl. Surf. Sci.*, 2017, **391**, 645–653.
24 D. Xu, B. Cheng, J. Zhang, W. Wang and J. W. Ho, *J. Mater. Chem. A*, 2015, **3**, 20153–20166.
25 X. He, J. Wang, Z. Shu, A. Tang and H. Yang, *RSC Adv.*, 2016, **6**, 41765–41771.
26 D. Xu, Y. Hai, X. Zhang, S. Zhang and R. He, *Appl. Surf. Sci.*, 2017, **400**, 530–536.
27 R. He, J. Zhang, J. Yu and S. Cao, *J. Colloid Interface Sci.*, 2016, **478**, 201–208.
28 B. Luo, D. Xu, D. Li, G. Wu, M. Wu, W. Shi and M. Chen, *ACS Appl. Mater. Interfaces*, 2015, **7**, 17061–17069.
29 A. Takai and P. Kamat, *ACS Nano*, 2011, **5**, 7369–7376.
30 Y. Shahar, F. Scotognella, I. Kriegel, L. Moretti, G. Cerullo, E. Rabani and U. Banin, *Nat. Commun.*, 2016, **7**, 10413.
31 S. Linic, P. Christopher and D. Ingram, *Nat. Mater.*, 2011, **10**, 911–921.
32 Z. Tong, D. Yang, Y. Sun and Z. Jiang, *RSC Adv.*, 2015, **5**, 56913–56921.
33 Z. Bao, X. Xu, G. Zhou and J. Hu, *Nanotechnology*, 2016, **27**, 305403.
34 X. Li, L. Wang, D. Xu, J. Lin, P. Li, S. Lin and W. Shi, *CrystEngComm*, 2015, **17**, 2421–2428.
35 X. Xu, Z. Bao, G. Zhou, H. Zeng and J. Hu, *ACS Appl. Mater. Interfaces*, 2016, **8**, 14118–14124.
36 G. Zhou, X. Xu, T. Ding, B. Feng, Z. Bao and J. Hu, *ACS Appl. Mater. Interfaces*, 2015, **7**, 26819–26827.